Channeling Acceleration by X-Rays in Crystals and Carbon Nanotubes

Young-Min Shin[a),b)], Dean A. Still[b)], and Vladimir Shiltsev[b)]

[a)]Northern Illinois Center for Accelerator and Detector Development (NICADD), Department of Physics, Northern Illinois University, Dekalb, IL, 60115, USA

[b)]Fermi National Accelerator Laboratory , Batavia, IL, 60510, USA

Acceleration of particles channeling in a crystal by means of diffracted x-rays via Bormann anomalous transmission was conceived for heavy ions and muons by Tajima and Cavenago [1], which potentially offers an appreciably high field gradient on the order of GV/cm. The theoretical model of the high gradient acceleration has been studied in two kinds of atomic structure, crystals and carbon nanotubes (CNTs), with analytic calculations and electromagnetic eigenmode simulations. A range of acceleration gradients and cutoffs of the x-ray power (the lowest power limit to overcome the Bremsstrahlung radiation losses) are characterized in terms of the lattice constants, unit cell sizes, and photon energies. The parametric analysis indicates that the required x-ray power can be reduced to an order of megawatt by replacing crystals with CNTs. Eventually, the equivalent dielectric approximation of a multi-wall nanotube shows that 250 ~ 810 MeV muons can be synchronously coupled with x-rays of 0.65 ~ 1.32 keV in the accelerating structure.

Operated by Fermi Research Alliance, LLC under Contract No. De-AC02-07CH11359 with the United States Department of Energy.

I. INTRODUCTION

Accelerating electrons and positrons to ultra-high energies beyond the tera-electron volt (TeV) scale within a reasonable footprint and with acceptable energy conversion efficiency has been a great challenge due to the particle radiation losses in the focusing channels and huge spread of the center-of-mass (COM) energies in short bunches induced at the interaction point of such e+e- colliders. Heavier particles like muons do not suffer from the radiation loss and nuclear interactions with either plasmas or solids and therefore seem to be more attractive for acceleration to ultra-high energies. A compact circular geometry with the heavy particle acceleration concept may enable the COM energy to reach a multi-TeV scale within existing accelerator facilities [2 – 4]. However, muons have a very short lifetime, which requires a fast acceleration to high COM energy before the muon decays into an electron, a neutrino and an antineutrino. Feasible concepts for high gradient acceleration are typically classified into three main categories depending upon types of acceleration media such as solid state structure, plasma, and crystal, which have been actively investigated [5]. It is well known that plasma-wakefield acceleration (PWA) offers the highest acceleration gradient, the order of $E_0 = m_e c \omega_p / e \approx 100 \times n_0^{1/2}$ [eV/m], where n_0 is the ambient plasma density [6].

However, the density of charge carriers (conduction electrons, $n_0 \sim 10^{22\,-\,23}$ cm^{-3}) in solids is even 4 ~ 5 orders of magnitude higher than those in a gaseous plasma. Particles passing through crystals in arbitrary direction can readily escape from the driving field due to fast pitch-angle diffusion resulting from increased scattering rates. It was thus suggested that particles are accelerated along major crystallographic directions. The ions and photons

are readily confined in the atomic tunnel of an angstrom-scale aperture, which is called the channeling effect. In principle, a crystal channel can hold an equivalent accelerating field of 10^{13} V/cm transverse and 10^{9} V/cm longitudinal electric fields of diffracted traveling EM-waves that are ideally applicable to fast acceleration. The major challenge of this channeling acceleration is that ultimate acceleration gradients require photon energies in a hard x-ray regime ($\hbar\omega \approx 40$ keV), exceeding those conceivable for x-rays sources as of today [7], though x-ray lasers can efficiently excite solid plasma and accelerate particles inside a crystal channel. Moreover, only disposable crystal accelerators in fibers or films can be used at such high externally driven fields. It will exceed the ionization thresholds and destroy the atomic structure, only allowing channeling acceleration to occur in a short time before full dissociation of the crystal lattice [8].

Particle channeling in crystal has been already successfully used in high energy beams for applications such as collimation, bending, and volume refraction [9, 10]. There were some previous studies of replacing crystals with the nano-structures that have a much wider range of flexibility and superior physical strength [11, 12]. In particular, carbon nanotubes (CNTs) have various advantages for channeling acceleration. First, the size of the CNT channel is readily controllable up to the sub-micron scale which can mitigate x-ray constraints required for channeling acceleration. Second, the larger size of the unit-cell can also decrease the de-channeling rates and increase the acceptance angles. Third, it enables three-dimensional beam control over a greater bending length. CNTs are comprised entirely of *sp*2 bonds, which are thermally and mechanically stronger than crystals, steels, and even diamonds (*sp*3 bond). Also, nanotubes have a higher probability of surviving in extremely

intense channeling, radiation, and acceleration interactions. This paper presents a theoretical analysis of x-ray channeling acceleration in crystals and CNTs with respect to structural dimensions. We also study the muon channeling acceleration conditions in a multi-wall nanotube by analytic calculations and simulations in an equivalent dielectric approximation (Drude model).

II. SYSTEM DESCRIPTION

X-ray channeling acceleration was well described in Ref. [1], including a theoretical model of beam-wave synchronization conditions. Looking back to the acceleration system, Figure 1 shows that an x-ray incident to a crystal with a Bragg angle undergoes anomalous optical transmission (Bormann effect) [11, 12] inducing x-ray diffraction among inter-planar lattice spaces. Channeling particles coupled in the same orientation can be accelerated by the guided traveling waves at the m^{th} diffraction order where they are synchronized with a periodicity of a superlattice with a Brillouin wave number $k_s = 2\pi/s$ where s is the periodic length, i.e. $\omega/(k_z + k_s) = c$, where ω and k_z are the light frequency and longitudinal wave number. As channeled particles are confined to the rows of atoms by electric fields of the order 1 — 10 V/Å, crystals can be used in a collider not only for acceleration sections but also for bending sections. In the channeling acceleration process, the Bormann effect must occur to hold strong inter-planar fields in the crystallographic planes and the transmission becomes stronger with a thicker crystal, as depicted in Fig. 1(b). Figures 1(c) and (d) are the electromagnetic wave transmission analysis results of a crystal model using a time-transient S-parameter solver. In our simulation, the crystal plate is

modeled with a lattice constant of 3.1 Å and a Bragg angle of 2.866°, designed from a coupling condition of the 10^{th} diffraction order. The incident plane wave slant to the crystal face forms tilt wave-fronts with respect to crystal orientation. It creates the longitudinal and transverse electric field components in the lattice spaces. The field plot depicts that transverse fields of the diffracted waves are a few orders of magnitude larger than longitudinal fields. Figure 1(d) is the normalized transmission of two crystal plate structures depicting 4 and 10 lattice layers. In the transmission spectrum, resonant diffraction peaks appear at the wavelengths corresponding to the Bragg angles. The simulation shows the Bormann effect occurring in the crystal for the 10-layered plate has a much stronger transmission than the 4-layered one. Figure 2 shows 3D plots of the anomalous transmission condition (required photon energy), obtained from $E_v = hc/2a/\sin\theta_B$ (h is thePlanck constant) in terms of a lattice constant, a, and Bragg angles, θ_B. It clearly shows that the required photon energy for the transmission can be significantly lowered with a larger lattice constant and a larger angle. In Fig. 2, increasing the size of the unit cell from 3 to 15 Å drops the x-ray energy down to an order of 0.1 ~ 10 keV, depending upon the Bragg angle. Enlarging a unit cell to the nano-scale can take the energy level of the driving photon source down to the ultraviolet or even the visible light spectrum. With the analytic calculation on radiation losses and x-ray powers, we extensively examined the channeling acceleration condition mainly with respect to their unit cell sizes and lattice constants.

III.THEORETICAL EVALUATION

Figure 3(a) illustrates a conceptual drawing of a crystal and a CNT showing the

dimensional parameters. In the analysis of a face-cubic centered (FCC) structure like silicon, a unit-cell is defined with the lattice constant, a, which is the atom-to-atom spacing. However, in the CNT model, a unit cell is specified by a tube of radius, R, and length l, which are a function of the lattice constant (c-c binding length). This analysis will consider the armchair structure. To properly accelerate particles in a crystal not only will the acceleration energy gain exceed the radiation loss, but it must also be less than the atomic binding energy (damage threshold). Therefore, the minimum channeling acceleration gradient (cutoff) is determined by the Bremsstrahlung radiation loss, $E_R = E_l/\lambda_R$, where E_l is the total energy loss over the radiation loss length, λ_R, [1], [8],

$$\lambda_R^{-1} = 4Z_{eff}^2 r_p^2 r_e^{-3} \alpha^7 \phi^{-3} K_0\left(\frac{2\pi r}{b}\right) \ln\left(\frac{2\gamma\alpha m_e}{m_p}\right), \tag{1}$$

and the maximum gradient (damage threshold) of atomic field, $E_B = e(E_b)_{max} R_1$, where E_b,

$$eE_b < mc\omega\alpha\sqrt{\frac{L_{min}}{a_B}}, \tag{2}$$

is obtained from $F_p < F_b$ (F_p: transverse focus force on the electron, F_b: electron binding force to the atom). Here, $r_p = e^2/m_p c^2$ is the classical radius of a particle with mass m_p (r_e for electron), $\phi = b/a_B$ (b: transverse lattice constant, $b = a$ for crystals), α is the fine-structure constant, a_B is the Bohr radius, K_0 is the modified Bessel function of the second kind, L is the transverse dimension of the x-ray beam (L_{min}: minimum dimension), ω is the angular frequency of x-ray photon, and R_1 is the longitudinal coupling ratio (R_l) of the 1st satellite [1].

Figure 3 (b) is the maximum acceleration gradient (eE_z) versus photon energy

(wavelength) with respect to the lattice constant (a) that can be provided by a crystal (below the damage threshold). The lower cutoffs of the highest gradient curves are restricted by the radiation loss. The lower cutoffs are calculated with the condition that the atomic number, Z, is 30, the effective charge, Z_{eff}, is 10, the superlattice constant ratio (s/a) is 20, the transverse mode number (N) is 2, and number of atoms in a unit cell is 1.5. Also, we assume that 1 TeV of particle energy is lost over the radiation loss length (total energy loss (E_l) = 1 TeV) and channeling muons (μ-) of $\beta \cong 0.995$ and $\gamma \cong 10$ is distributed in the transverse atomic space of 0 ~ $a/2$. With this condition, the acceleration gradients of crystals with a = 1.5 ~ 4.0 Å are calculated with a photon energy of 0.2 ~ 41.34 keV (0.3 ~ 62.2 Å). Figure 3 shows the result that a smaller unit cell leads to a higher field gradient. Note that the smaller lattice structure increases the cutoff of the acceleration gradient as particles lose more energy by radiation at wavelengths comparable to the structure dimensions. Figures 3(c) and (d) show the maximum acceleration gradient (upper limit) versus the photon energy for two CNT models where a = 1.5 Å and 2.5 Å (Z = 6). The unit cell volume of a single-wall tube is defined as $V_{cnt} = \pi R^2 l$, where R and l is the radius and length of the tube unit cell respectively. These are determined by the number of c_6-cells (honeycombs) in the circumference. In general, expressions $R_{armchair} = \frac{n_{cnt}(3a)}{2\pi}$ and $l_{armchair} = \sqrt{3}a$ describe the armchair and expressions $R_{zigzag} = \frac{n_{cnt}(\sqrt{3}a)}{2\pi}$ and $l_{zigzag} = 3a$ describe the zigzag, where n_{cnt} is the number of the c_6-cells along the tube circumference. The expressions correspond to unit-cell volumes $V_{armchair} = \frac{9\sqrt{3}}{4\pi} n_{cnt}^2 a^2$ and $V_{zigzag} = \frac{9}{4\pi} n_{cnt}^2 a^2$.

Therefore, the armchairs are about 73% larger than the zigzags with the same number of c_6-cells. The plasma density of a single-wall nanotube (SWNT) is given by $n_{cnt} = N_{cnt}/V_{cnt}$, where N_{cnt} is the number of the ions and their inner-shell electrons in a tube unit-cell. The graphs are plotted with the 3 to 15 c_6-cells along the circumference (R = 2.15 ~ 10.75 Å with a = 1.5 Å and R = 3.58 ~ 17.9 Å with a = 2.5 Å). The upper thresholds of accelerating gradients with a = 1.5 Å and a = 2.5 Å are reduced to ~ 15 % for the crystal (silicon, Fig. 3(b)). This corresponds to an acceleration gradient of E_{acc} = ~ 150 MeV/cm (a = 1.5 Å) and = ~ 70 MeV/cm (a = 2.5 Å). The reduction of the acceleration gradient is mainly owing to the smaller atomic number, Z, and larger unit-cell size of CNTs. It should be noted that the cutoff acceleration gradient significantly drops with smaller radiation losses for muons owing to the larger beam tunnel and lower plasma density.

The damage threshold which limits the power density below the structural destruction is defined as $\rho_{threshold} = E_b^2/Z_0$, where Z_0 is the impedance of vacuum a meter (= 120π). Figure 4 is a plot of the power density thresholds versus the photon energy for a crystal in Fig. 4(a) and a CNT in Fig. 4(b) with respect to lattice constants. In particular, we assumed that for the nanotubes the damage threshold is only determined by the lattice constants without the need for considering the radius R and the length l as the lattice of the tubes would be disassociated if a c_6-cell is destroyed. Similarly as plot in Fig. 3, the x-ray power density, which is smaller than the radiation loss (cutoff), is not represented in the graphs because the x-ray will destroy the structure before channeled particles gain a sufficient amount of energy from the x-ray to overcome the energy loss if the cutoff of x-ray power density is larger than the damage threshold. The calculation indicates that the damage threshold of the

crystal is larger than the cutoff over the x-ray regime of $\geq \sim 2.32$, while the loss effect dominantly appears below ~ 2.32 keV, which limits the threshold above 0.1 ~ 5.3 W/Å^2 over 0.2 ~ 2.32 keV. On the other hand, as shown in Fig. 4(b), the tubes have a lower threshold due to the relatively lower charge carrier density (Z = 30 → 6), which is higher than the cutoff (radiation power loss) over the same x-ray energy regime.

Figure 5 depicts the summarized graphs of the (a) cutoff gradients and (b) the upper gradient threshold of the crystal and the CNTs with respect to the tube unit-cell sizes. As shown in Fig. 5(a), CNTs and crystals have similar levels of energy loss within the same range of the unit cell dimension, but the cutoff appears significantly smaller with the larger tube unit-cell size. Note that the upper acceleration limit from the structural damage threshold is also lowered with the larger unit-cells due to the lower density. Figure 6 shows the lower limit of x-ray power density versus unit-cell size curve, obtained from Fig. 5(a). It should be stressed that replacing a crystal with a nanotube lowers the cutoff of required power by three orders of magnitude, which reduces the maximum acceleration gradient from 0.36 (4 Å) – 1.52 (1.5 Å) GeV/cm of crystal (Z = 30) to 0.15 GeV/cm (a = 1.5 Å) and 0.07 GeV/cm (a = 2.5 Å) of CNTs with a few nanometers of tube unit cell dimension. The analysis result shows that CNTs can significantly lower the power level required for x-ray channeling acceleration.

IV. NUMERICAL ANALYSIS

Expanding the analysis beyond the theoretical calculations, the acceleration condition in a nanotube can be estimated with simulation based on a finite-integration-technique (FIT). For this simulation, a multi-wall nanotube is designed with an equivalent dielectric medium

that contains three layers, as illustrated in Fig. 7(a). A single-wall and double-wall nanotube does not support the condition of a confined slow wave mode at the spectral band. Figure 7(b) shows a 3D-plot of the electrostatic potential distribution where 140 V is used for the atom-to-atom space across the cross-section of the triple-wall nanotube. The nanotubes are anisotropic media with different effective dielectric constants depending upon the tube orientation [13 – 15]. The tube is thus modeled with the three layered dielectric rod of $\varepsilon_{\parallel}$ = 31.87 and $\varepsilon_{\perp}$ = 39.21 with $\sigma_{\parallel}$ = 69.54 and $\sigma_{\perp}$ = 178.65 ($\varepsilon = \varepsilon' + i\frac{\sigma}{\omega\varepsilon_0}$, where ε' = $\varepsilon_{\parallel}$ or $\varepsilon_{\perp}$ and σ = $\sigma_{\parallel}$ or $\sigma_{\perp}$). Figure 7(c) represents the dispersion curve (energy band diagram: photon energy versus wave constant) of the confined slow wave modes (inset in Fig. 7(d)), obtained from eigenmode simulations with a = 1.4 Å and R = 14 Å. The synchronized photon-muon coupling condition in the designed tube provides the energy ranges of the x-ray and the muon beam for channeling acceleration: 0.65 ~ 1.32 keV for x-rays and 250 ~ 810 MeV for muon beams. The eigenmode simulation analysis is programmed with the condition that assigns a *k*-vector (fundamental mode) normal to the master and slave ports of the periodic boundaries, which imposes a polarization of the electric fields perpendicular to the tube orientation at the port boundaries. With this condition, transverse fields appear more dominant than longitudinal fields on the confined modes along the wave vectors. However, in practice EM waves should be incident to an acceleration structure with a Bragg angle for longitudinal coupling, so the grazing incidence accommodates longitudinal field components in the tube and the ratio between the transverse and longitudinal fields widely varies with respect to the incident angle; i.e. the longitudinal coupling ratio, R_l, has a

strong dependence with an incident angle. The numerical analysis with the simulation modeling corroborates the theoretical calculation results presented in section-III. The extended proof of concept may include comprehensive modeling with particle-tracking and particle-in-cell (PIC) simulations. The extended simulation analysis and experimental test are currently under development, which will be discussed elsewhere.

V. CONCLUSION

A theoretical analysis that is presented in Ref. [1] has been applied to the structure parameters of crystals and CNT's where x-ray channeling acceleration is known to provide a GeV/cm level of acceleration gradient. It turns out that nanotubes can significantly lower the cutoff of the x-ray power required for the acceleration energy gain by a few orders of magnitude. Lowering the cutoff is also accompanied by a reduction of the acceleration gradient to 5 ~ 10% due to an increase in the unit-cell size. The result shows that the large reduction of the required x-ray power level by employing nano-structures turns the channeling photon interactions with heavy particles, i.e. muons and protons, into a more viable approach for extremely high gradient acceleration with power levels from currently existing coherent x-ray sources. A wide scope of theoretical and experimental studies on the idea is currently underway.

ACKNOWLEDGEMENT

The work was supported by the Fermi Research Alliance, LLC under the U.S. Department of Energy.

REFERENCES

[1] T. Tajima, M. Cavenago, *Phys. Rev. Lett.* **59** 1440 (1987)

[2] V. Shiltsev, *Mod. Phys. Lett. A* **25** 567 (2010)

[3] *The Neutrino Factory Int'l Scoping Study Accelerator Working Group Report, JINST* **4** P07001 (2009)

[4] A. Poklonskiy, D. Neuffer, *Int. J. Mod. Phys*. **A24** 959 (2009)

[5] W. Gai, in AIP *Conf. Proc.* **1086** 3 (2008)

[6] W. Leemans, *ICFA Beam Dynamics Newsletter* **56** 10 (2011)

[7] A. Caldwell, K. Lotov K, A. Pukhov, F. Simon, *Nature Phys.* **5** 363 (2009)

[8] P. Chen, R. Noble, *AIP Conf. Proc.* **398** 273 (1997)

[9] Biryukov V, Chesnokov Yu, Kotov V *Crystal Channeling and Its Application at High Energy Accelerators* (Springer–Verlag, Berlin, Heidelburg, 1997)

[10] Mokhov N, *et. al.*, *JINST* **6** T08005 (2011)

[11] V. M. Biryukov, S. Bellucci, *Nuclear Instruments and Methods in Physics Research B* 234 (2005) 99–105

[12] S. Bellucci, Nuclear Instruments and Methods in Physics Research B 234 (2005) 57 – 77

[13] B. W. Batterman and H. Cole, Rev. Mod. Phys. 36, 681 (1964)

[14] P. O. Ewald, Fifty Years of X Ra-y Diffraction (International Union of crystallography, Utrecht, 1962), 249

[15] Anestis Katsounaros, Khalid Z. Rajab, Yang Hao, Mark Mann, and William I. Milne, Appl. Phys. Lett. **98**, 203105 (2011)

[16] A. Katsounaros, M. Mann, M. Naftaly, K.Z. Rajab, Y. Hao, W.I. Milne, *Carbon* 50 (3), 939 (2012)

[17] Anestis Katsounaros, “Characterization of Multi-Wall Carbon Nanotubes and their Applications”, PhD Thesis of School of Electronic Engineering and Computer Science, Queen Mary, University of London

FIGURE CAPTIONS

FIG. 1 (a) Conceptual drawing of x-ray channeling acceleration (muons) (b) transmission spectra of thin and thick crystals in Bormann effect (anomalous transmission) (c) 2D-contour plot of diffracted electric field distribution in the Bormann effect at $\theta_B \sim 2.866°$, obtained from EM-wave simulation (d) simulated transmission spectra of crystals with 4- and 10-lattice layers

FIG. 2 3D-plots of Bormann effect condition, calculated from $E_v = hc/2a/\sin\theta_B$. Bragg angle, lattice constant, versus photon energy plots of (a) $a = 1 \sim 15$ Å and (b) $a = 1 \sim 10^4$ Å

FIG. 3 (a) Conceptual drawings of a crystal (silicon) and a CNT with dimensional parameters. Maximum gradients versus photon energy graphs of (b) crystals and CNTs of (c) $a = 1.5$ Å and (d) $a = 2.5$ Å

FIG. 4 Upper limit of x-ray power (damage threshold) versus photon energy graphs of (a) crystals and (b) CNTs

FIG. 5 (a) Minimum acceleration gradient (cutoff) and (b) upper limit (damage threshold) of acceleration gradient versus unit-cell size graphs of a crystal (Z = 30) and CNTs (Z = 6), $a = 1.5$ Å and $a = 2.5$ Å.

FIG. 6 Minimum acceleration gradient (cutoff) and (b) upper limit (damage threshold) of

acceleration gradient versus unit-cell size graphs of a crystal and CNTs

FIG. 7 (a) 3-wall CNT model (b) electrostatic potential (V_{max} = 140 eV) (c) dispersion curve of transverse CNT-mode and muon beam line (~ 420 MeV), and (d) synchronized muon versus x-ray energy graph in the CNT

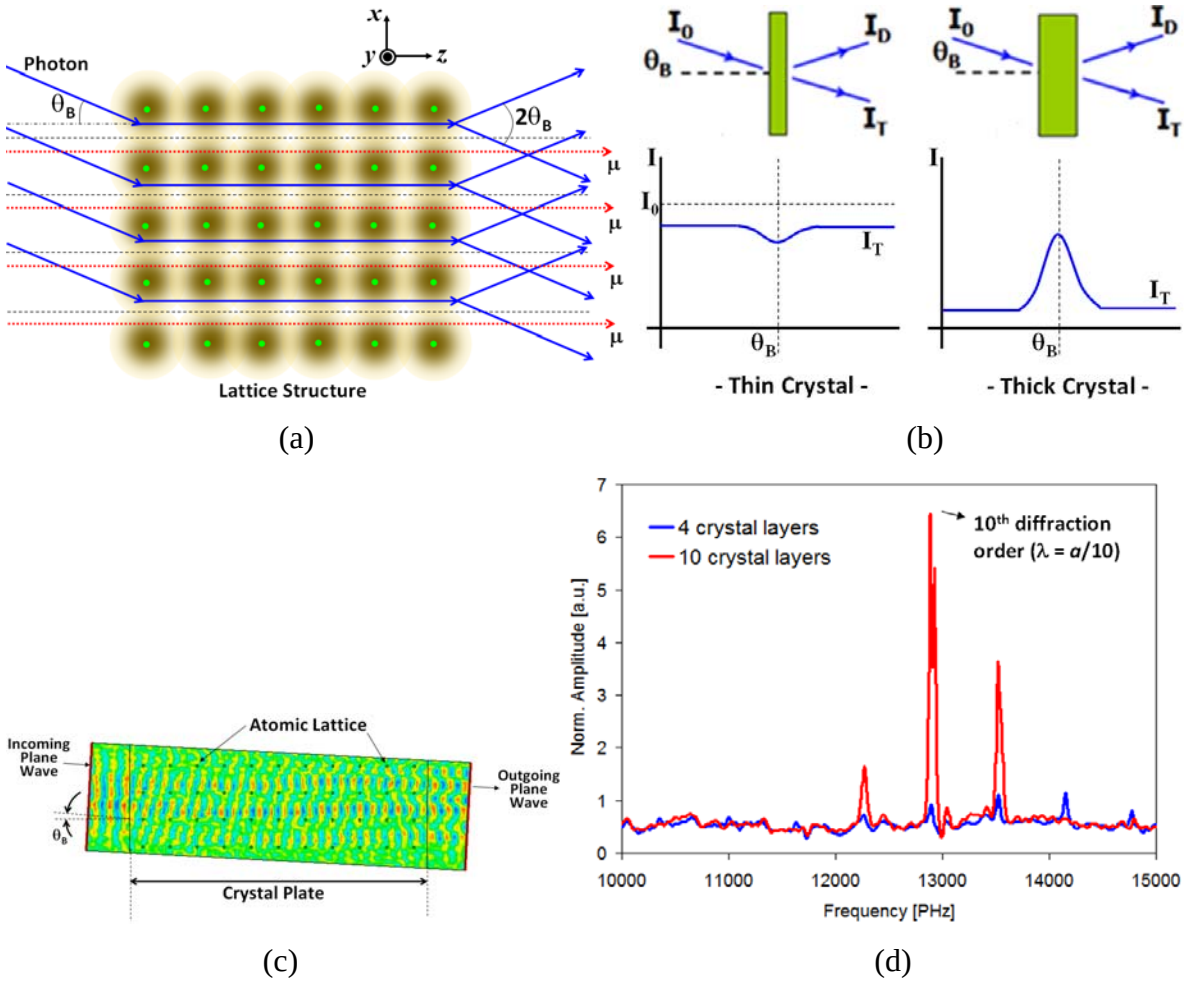

FIG. 1 (Y. M. Shin)

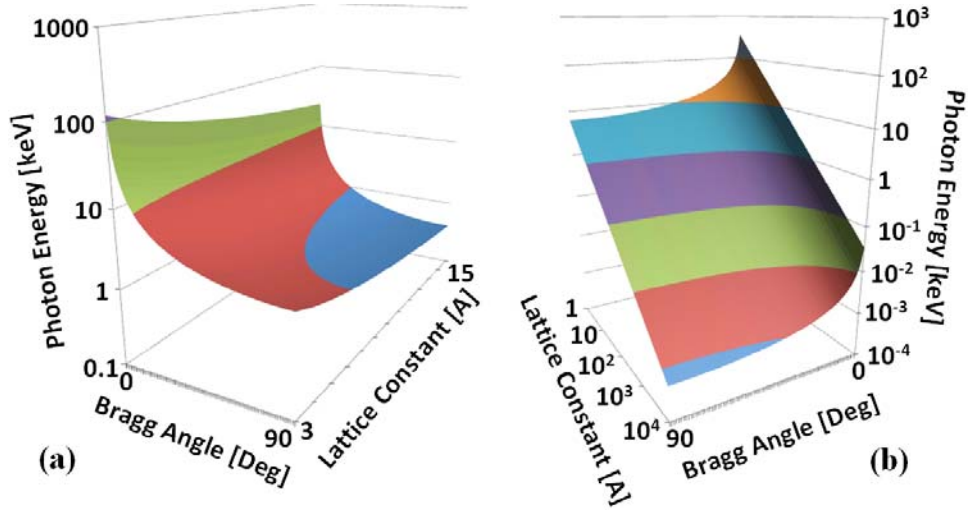

FIG. 2 (Y. M. SHIN)

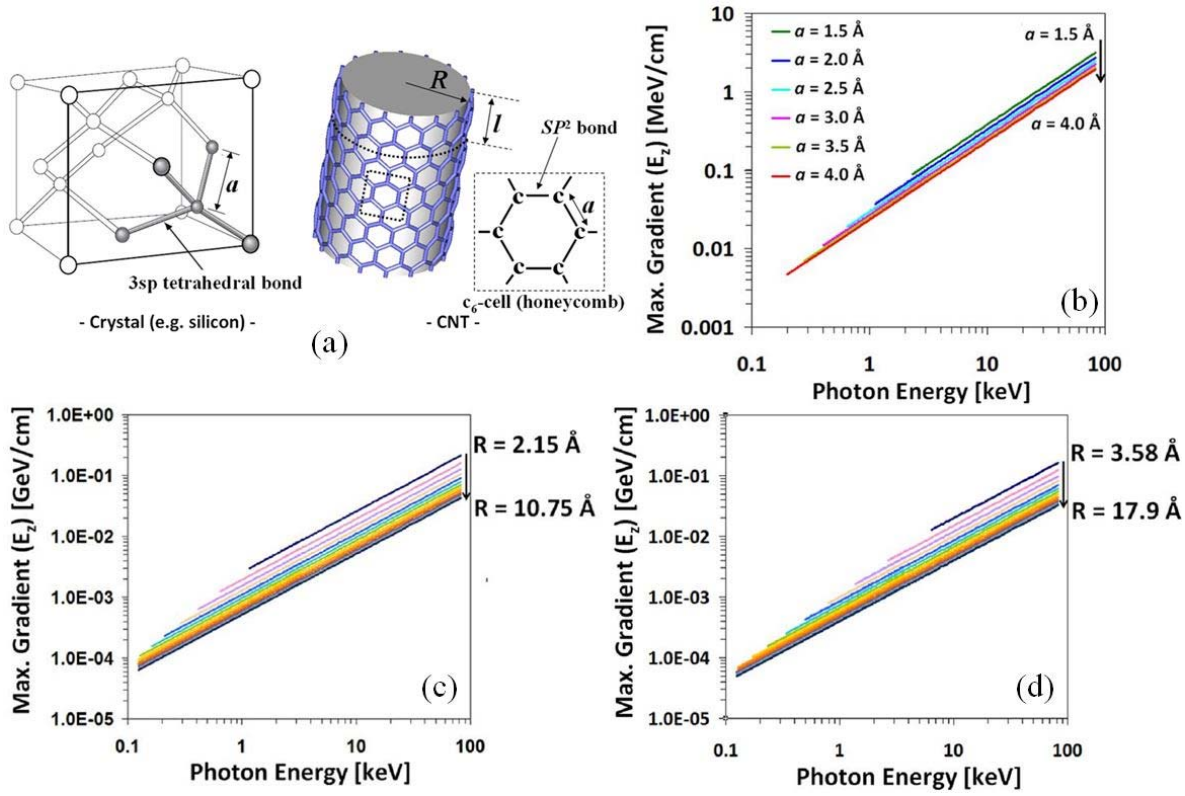

FIG. 3 (Y. M. SHIN)

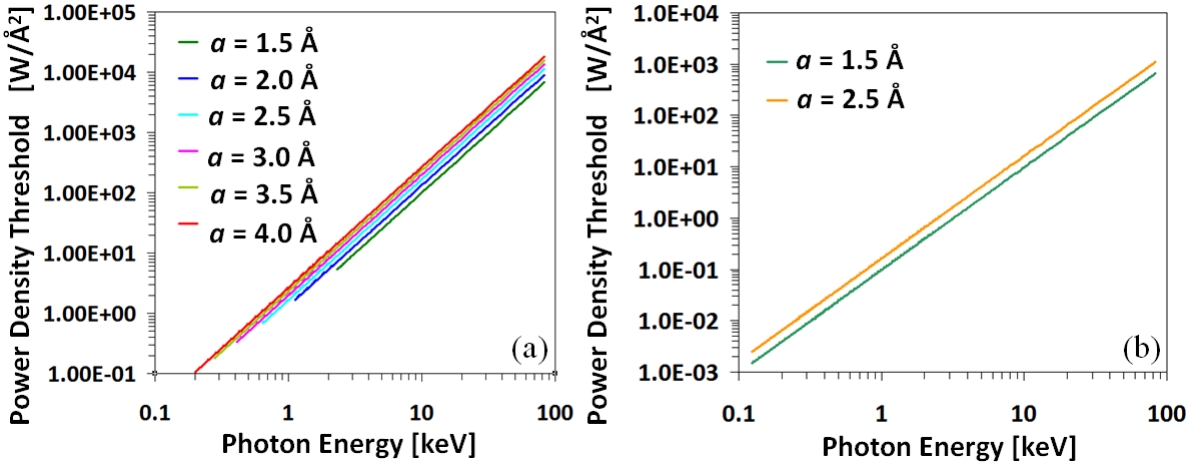

FIG. 4 (Y. M. SHIN)

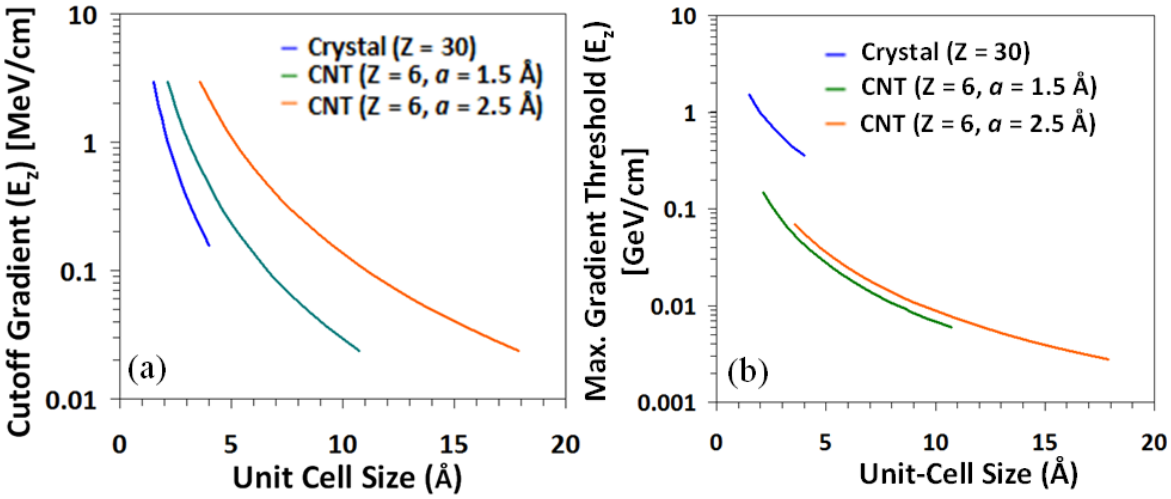

FIG. 5 (Y. M. SHIN)

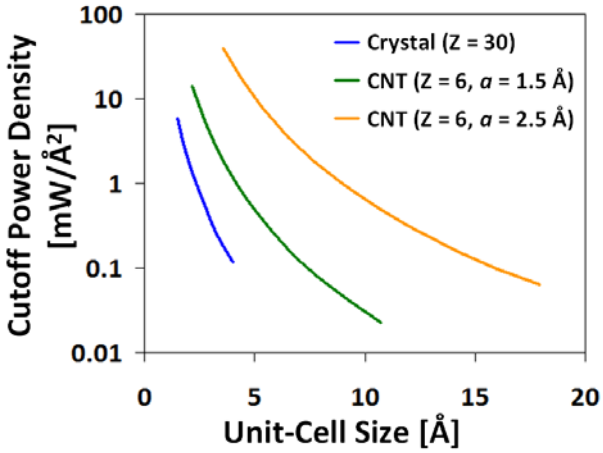

FIG. 6 (Y. M. Shin)

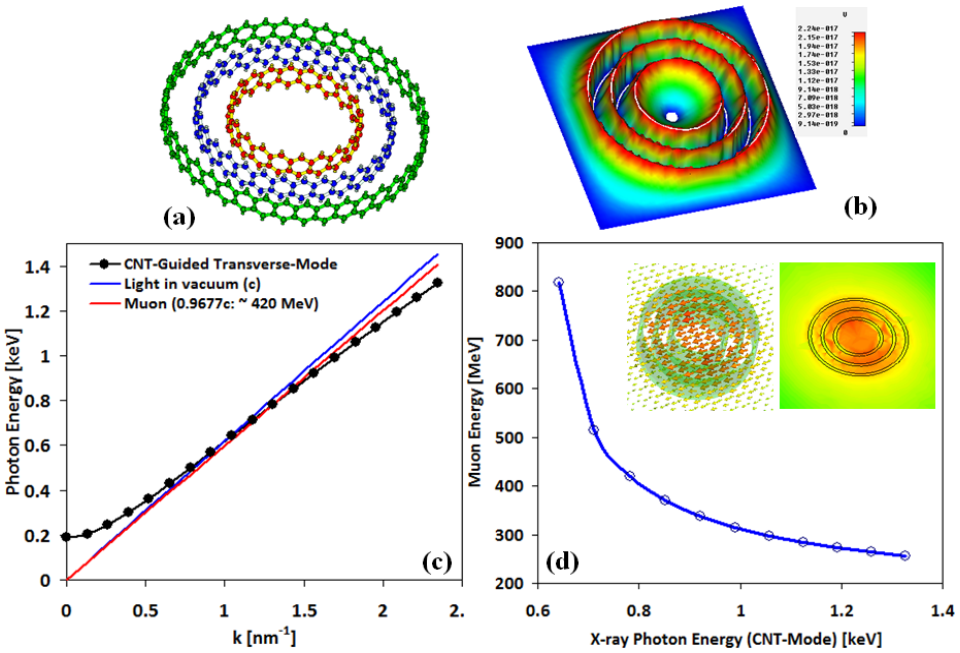
(a)
(b)
CNT-Guided Transverse-Mode
Light in vacuum (c)
Muon (0.9677c: ~ 420 MeV)
Photon Energy [keV]
k [nm^{-1}]
(c)
Muon Energy [MeV]
X-ray Photon Energy (CNT-Mode) [keV]
(d)

FIG. 7 (Y. M. Shin)